Journal of Alloys and Compounds 782 (2019) 632–640

Contents lists available at ScienceDirect

Journal of Alloys and Compounds

journal homepage: http://www.elsevier.com/locate/jalcom

# Solid-state synthesis and characterization of ferromagnetic $Mn_5Ge_3$ nanoclusters in GeO/Mn thin films

V.G. Myagkov [a], A.A. Matsynin [a, *], L.E. Bykova [a], V.S. Zhigalov [a], Yu.L. Mikhlin [b], M.N. Volochayev [a, c], D.A. Velikanov [a], A.S. Aleksandrovsky [a, d], G.N. Bondarenko [b]

[a] Kirensky Institute of Physics, Federal Research Center KSC SB RAS, Russian Academy of Sciences, Krasnoyarsk, 660036, Russia
[b] Institute of Chemistry and Chemical Technology, Federal Research Center KSC SB RAS, Russian Academy of Sciences, Krasnoyarsk, 660036, Russia
[c] Siberian State Aerospace University, Krasnoyarsk, 660014, Russia
[d] Institute of Nanotechnology, Spectroscopy and Quantum Chemistry, Siberian Federal University, Krasnoyarsk 660041, Russia

ARTICLE INFO

*Article history:*
Received 29 May 2018
Received in revised form
27 November 2018
Accepted 8 December 2018
Available online 12 December 2018

*Keywords:*
Mn-Ge system
Thin-film solid-state reactions
$Mn_5Ge_3$ alloy
Nowotny $Mn_5Ge_3O_y$ phase
Magnetic properties

ABSTRACT

$Mn_5Ge_3$ films are promising materials for spintronic applications due to their high spin polarization and a Curie temperature above room temperature. However, non-magnetic elements such as oxygen, carbon and nitrogen may unpredictably change the structural and magnetic properties of $Mn_5Ge_3$ films. Here, we use the solid-state reaction between Mn and GeO thin films to describe the synthesis and the structural and magnetic characterization of $Mn_5Ge_3(Mn_5Ge_3O_y)$-$GeO_2(GeO_x)$ nanocomposite materials. Our results show that the synthesis of these nanocomposites starts at 180°C when the GeO decomposes into elemental germanium and oxygen and the resulting Ge atoms immediately migrate into the Mn layer to form ferromagnetic $Mn_5Ge_3$ nanoclusters. At the same time the oxygen atoms take part in the synthesis of $GeO_x$ and $GeO_2$ oxides and also migrate into the $Mn_5Ge_3$ lattice to form $Mn_5Ge_3O_y$ Nowotny nanoclusters. Magnetic analysis assumes the general nature of the Curie temperature increase in carbon-doped $Mn_5Ge_3C_x$ and $Mn_5Ge_3O_y$ films. Our findings prove that not only carbon, but oxygen may contribute to the increase of the saturation magnetization and Curie temperature of $Mn_5Ge_3$-based nanostructures.



## 1. Introduction

In recent years, the synthesis features and structural, electronic and magnetic properties of ferromagnetic $Mn_5Ge_3$ films have been intensively studied for future applications in spintronics [1–5]. An important advantage of $Mn_5Ge_3$ is a sufficiently high spin polarization [6,7] and epitaxial growth on Ge(111) and Ge(001) substrates by solid-phase epitaxy [8–11]. Thus, in epitaxial $Mn_5Ge_3$/Ge(111) and $Mn_5Ge_3$/Ge(001) samples, the ferromagnetic $Mn_5Ge_3$ compound can potentially be used as a source of spin injection into the Ge layer [8–11]. $Mn_5Ge_3$ has Curie temperature only slightly above room temperature ($T_C = 304$ K), and a common method of increasing the Curie temperature is the doping of $Mn_5Ge_3$ by C, O [8,9,12,13]. For epitaxial $Mn_5Ge_3C_x$ films the Curie temperature increases with the carbon concentration and reaches a maximum $T_C = 460$ K at x ~0.6–0.7 [13]. The homogeneous distribution of oxygen and carbon in $Mn_5Ge_3$ films obtained in a vacuum of $10^{-6}$ Torr suggests that the increase in the Curie temperature and magnetization is due to the migration of C and O impurities to the $Mn_5Ge_3$ lattice and the formation of the Nowotny phase of $Mn_5Ge_3C_xO_y$ [14–16]. Experimental studies have shown that N, C and O impurities, which are present even in ultra-high vacuum, migrates into the Mn-Ge nanostructures during precipitation or annealing and change the magnetic and electrical properties [17–20]. Calculations show, as a result of the reactivity of manganese, that at high oxygen concentrations the structural and magnetic properties of Mn-doped germanium are greatly reduced or even suppressed [21]. However, the effect of oxygen on the chemical interaction of Mn with Ge is still poorly understood.

Herein, we report the synthesis of ferromagnetic $Mn_5Ge_3(Mn_5Ge_3O_y)$-$GeO_2(GeO_x)$ nanocomposite films containing ferromagnetic $Mn_5Ge_3$ and $Mn_5Ge_3O_y$ nanoclusters embedded into dielectric $GeO_2$ and $GeO_x$ matrices via a solid state reaction between the GeO and Mn layers. A schematic illustration of the reaction in the Mn/GeO bilayer after annealing up to 300°C is

* Corresponding author.
*E-mail address:* matsyninaa@gmail.com (A.A. Matsynin).

https://doi.org/10.1016/j.jallcom.2018.12.126
0925-8388/

presented in Fig. 1. Annealing studies of the Mn/GeO bilayers demonstrate the start of a reduction-oxidation reaction at 180°C, producing the decomposition of GeO into Ge and germanium oxides $GeO_2(GeO_x)$, along with a solid-state reaction between the Mn and Ge that occurs simultaneously. The final reaction products at 300°C are ferromagnetic $Mn_5Ge_3$ and $Mn_5Ge_3O_y$ nanoclusters embedded in a $GeO_2(GeO_x)$ matrix.

## 2. Experimental details

### 2.1. Sample preparation

The initial Mn/GeO films were obtained by the successive thermal deposition of the GeO and Mn layers onto 0.18 mm thick chemically pure glass substrates at a residual pressure of $10^{-6}$ Torr. Previously, the substrates were degassed at 350 °C for 1 h, which was followed by the deposition of the GeO layers at a temperature of 180 °C. The X-ray photoelectron spectroscopy (XPS) studies show the formation of highly stoichiometric GeO films by the thermal deposition method. The top Mn layer was deposited at room temperature to prevent a reaction between the Mn and GeO during the deposition. The nominal thicknesses obtained from cross-sectional transmission electron microscopy (TEM) were 100 nm for Mn and 300 nm for GeO (this structure is denoted as A-Mn/GeO further in the text). The Mn(50 nm)/GeO(100 nm) bilayers and Mn(20 nm)/GeO(30 nm) films on NaCl(001) were prepared for magnetic and TEM studies (B-Mn/GeO further in the text), respectively. Film thicknesses were determined by X-ray fluorescent analysis or cross-sectional TEM image. The TEM studies show the differences in structural changes between A-Mn/GeO and B-Mn/GeO during annealing up 300 °C.

### 2.2. Synthesis

The initial Mn/GeO bilayers were annealed at temperatures between 50 and 500 °C at 50 °C intervals. The samples were held at each temperature at a pressure of $10^{-6}$ Torr for 1 h. X-ray fluorescence (XRF) was used to determine the film thickness of the GeO and Mn film thicknesses and the volume fraction of Ge in the GeO film. This allowed us to estimate the full volume of the synthesized $Mn_5Ge_3$ nanoclusters after annealing in GeO/Mn films to find the saturation magnetization $M_s$ and the perpendicular anisotropy constant $K^{\perp}$.

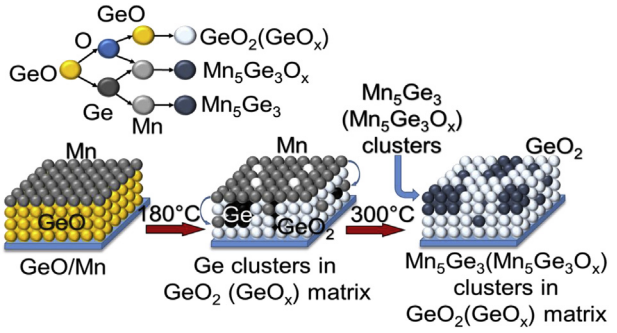


**Fig. 1.** Solid-state synthesis of $Mn_5Ge_3(Mn_5Ge_3O_y)$-$GeO_2(GeO_x)$ nanocomposites. (a) Schematic illustration of the synthesis of ferromagnetic $Mn_5Ge_3(Mn_5Ge_3O_y)$-$GeO_2(GeO_x)$ nanostructures by annealing the A-Mn/GeO bilayers up to 300 °C. Above the initiation temperature $T_{in}$ ~180 °C, GeO decomposes into elemental Ge and O. Simultaneously the Ge and O atoms migrate into the Mn layer for the synthesis of the ferromagnetic $Mn_5Ge_3(Mn_5Ge_3O_y)$ nanoclusters and Ge with O forms the $GeO_2(GeO_x)$ matrix.

### 2.3. TEM characterization

The cross-sectional samples for investigation by TEM were prepared using a focused ion beam (FIB, Hitachi FB2100) at 40 kV. During sample preparation, the tungsten layer was deposited on the surface of the film by the decomposition of gaseous $W(CO)_6$, in order to protect the surface of interest from milling by the Ga+ ion beam. TEM investigations were carried out using a Hitachi HT7700 TEM at 100 kV (W source) equipped with a scanning TEM system and a Bruker Nano XFlash 6T/60 energy dispersive X-ray (EDX) spectrometer. The obtained Mn/GeO and GeO films were separated from the substrate, placed on a molybdenum TEM grid and annealed at 300 °C for 1 h.

### 2.4. XPS studies

X-ray photoelectron spectra were collected using a SPECS instrument (Germany) equipped with a PHOIBOS 150 MCD 9 hemispherical analyzer at a pass energy of 20 eV for survey spectra and 8 eV for narrow scans. The Mg K-line (1253.6 eV) of a dual anode X-ray source was used for excitation. Sample etching with $Ar^+$ ions was performed with a PU-IQE 12/38 scanning source operated at an accelerating voltage of 5 kV and ion emission current of 15 μA, which corresponds to a scattering rate of ~1 nm/min. Surface concentrations of elements were determined from the survey spectra using the empirical relative sensitivity factors embedded in the CasaXPS program. The high-resolution spectra were fitted with Gaussian-Lorentzian peak profiles after Shirley background subtraction.

### 2.5. Magnetic and resistivity measurements

Saturation magnetization $M_s$ and Curie temperature $T_C$ measurements were performed on a vibration magnetometer with in-plane magnetic fields up to 2 kOe. We also measured the saturation magnetization $M_s$ and the perpendicular anisotropy constant $K\perp = 2\pi M_s^2 \pm \Delta K\perp$ using a torque magnetometer with a sensitivity of $3.76 \times 10^{-9}$ Nm in the applied field range of 0–18 kOe at room temperature. The value of $\Delta K\perp$ in thin films was associated with the presence of in-plane strains and grain growth textures [22,23].

## 3. Results

### 3.1. Solid state reactions in Mn/GeO bilayers

#### 3.1.1. Temperature characterization of solid-state reactions in Mn/GeO films

Fig. 2 shows the saturation magnetization $M_s(T_s)$ **(a)** and electrical resistance $R(T_s)$ **(b)** of the A-Mn/GeO bilayers as a function of annealing temperature $T_s$. Up to ~180 °C, the Mn/GeO samples remained nonmagnetic, which implies the absence of mixing and the formation of magnetic phases on the Mn/GeO interface (Fig. 2a). With an increase in the annealing temperature above ~180 °C, the saturation magnetization $M_s$ appears in the Mn/GeO films and reaches a maximum value after annealing at 300 °C. This clearly indicates the onset of a solid-state reaction above the initiation temperature $T_{in}$ ~180 °C between the Mn and GeO layers and the synthesis of one or more ferromagnetic phases. The volume fraction of these phases in the reaction products increases up to 300 °C. After annealing above 300 °C, the degradation of the ferromagnetic phases reduced the magnetization, which dropped to zero at 400 °C (Fig. 2a). Fig. 2b shows the temperature dependence of the electrical resistance $R(T_s)$ of the Mn/GeO film sample, which was heated at a rate of 4 °C/min to 500 °C and cooled to room temperature. The slow increasing of electrical resistance $R(T_s)$ above $T_{in}$ ~180 °C is

consistent with the start of the solid phase reaction between the Mn and GeO layers, which finished at 300 °C. After annealing at 350 °C the resistance $R(T_s)$ slowly decreased during cooling down to room temperature. The insignificant increasing of the resistance (about 2.5 times) and the metallic-like temperature dependence of $R(T_s)$ explicitly indicates that after annealing at 350 °C the A-Mn/GeO samples contains a residual Mn layer (inset in Fig. 2b). The strong growth of electrical resistance $R(T_s)$ above 350 °C is undoubtedly associated with the formation of a nonconducting matrix. At decreasing temperature from 500 °C to room temperature the resistance $R(T_s)$ increases, which is a typical feature of semiconductor samples (Fig. 2b).

The diffraction pattern of the starting Mn/GeO bilayers contained reflections from the Mn layer and did not change up to the initiation temperature $T_{in}$ ~180 °C (Fig. 3a). The absence of reflections from the GeO layer suggests amorphous or nanocrystalline growth. After annealing at 250 °C, reflections from the pure Mn decreased and reflections from the ferromagnetic $Mn_5Ge_3$ phase appear (Fig. 3b). The intensity of the $Mn_5Ge_3$ reflections increased up to 300 °C (Fig. 3c), began to reduce above 300 °C and vanished completely after annealing above 400 °C (Fig. 3d). The formation of the ferromagnetic $Mn_5Ge_3$ phase matches well with the occurrence of magnetization in the 180–300 °C temperature interval and disappears after annealing at 400 °C (Fig. 2a). The findings suggest that a disproportionation reaction (1), producing Ge nanoclusters embedded into a $GeO_2$ matrix and a solid-state reaction between Ge and Mn (2) simultaneously start in the Mn/GeO interface above 180 °C and completely finish after annealing at 300 °C.

$$2GeO \rightarrow Ge^0 + GeO_2 \quad (1)$$

$$3Ge^0 + 5Mn \rightarrow Mn_5Ge_3 \quad (2)$$

The disproportionation reaction (1) of $GeO_x$ into elemental $Ge^0$ and $GeO_2$ composite obtained by vacuum annealing is commonly used in Ge nanostructure synthesis [24–26]. Above 300 °C new peaks of Ge and MnO appeared in addition to the $Mn_5Ge_3$ reflections and became dominant peaks above 400 °C (Fig. 3d and e). This suggests the structural degradation of ferromagnetic $Mn_5Ge_3$ by oxidation of Mn above 300 °C and as a result the phase separation of $Mn_5Ge_3$ into elemental $Ge^0$ and MnO nanoclusters.

Thus, magnetic, resistance and X-ray studies designated two temperature features: the initiation temperature of the reaction between Mn and GeO is $T_{in}$ ~180 °C and the oxidation of Mn in $Mn_5Ge_3$ nanoclusters, which is contained in the reaction products, occurs in the 300–500 °C temperature interval.

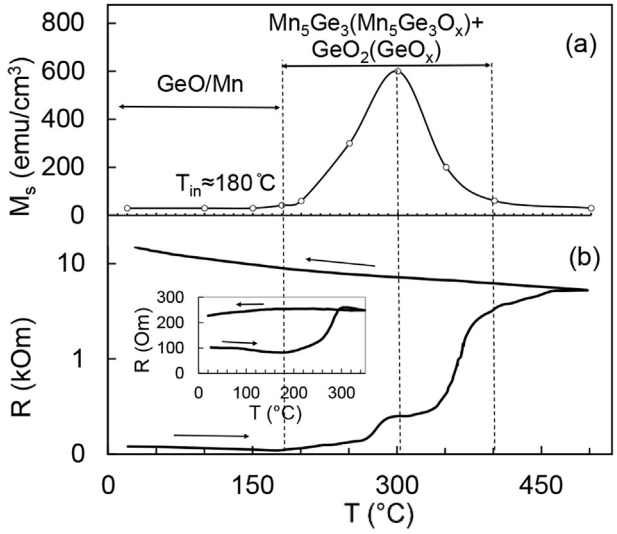


**Fig. 2.** Determination of the initiation temperature $T_{in}$ ~180 °C of the reaction between the Mn and GeO layers. (a) The saturation magnetization $M_s$ of the A-Mn/GeO bilayers as a function of annealing temperature $T_s$. The synthesis of the ferromagnetic $Mn_5Ge_3(Mn_5Ge_3O_y)$ nanoclusters in the Mn/GeO bilayers starts at $T_{in}$ ~180 °C and above 300 °C the Mn oxidation inhibits the magnetism in the sample. (b) Electrical resistance of the A-Mn/GeO bilayers heated up to 500°C and cooling to room temperature as a function of the temperature measurement $T_s$. The inset shows the $R(T_s)$ of the Mn/GeO bilayers heated up to 300°C and then cooled to room temperature. The metallic resistance is a consequence of the unreacted Mn layer on the top of the sample.

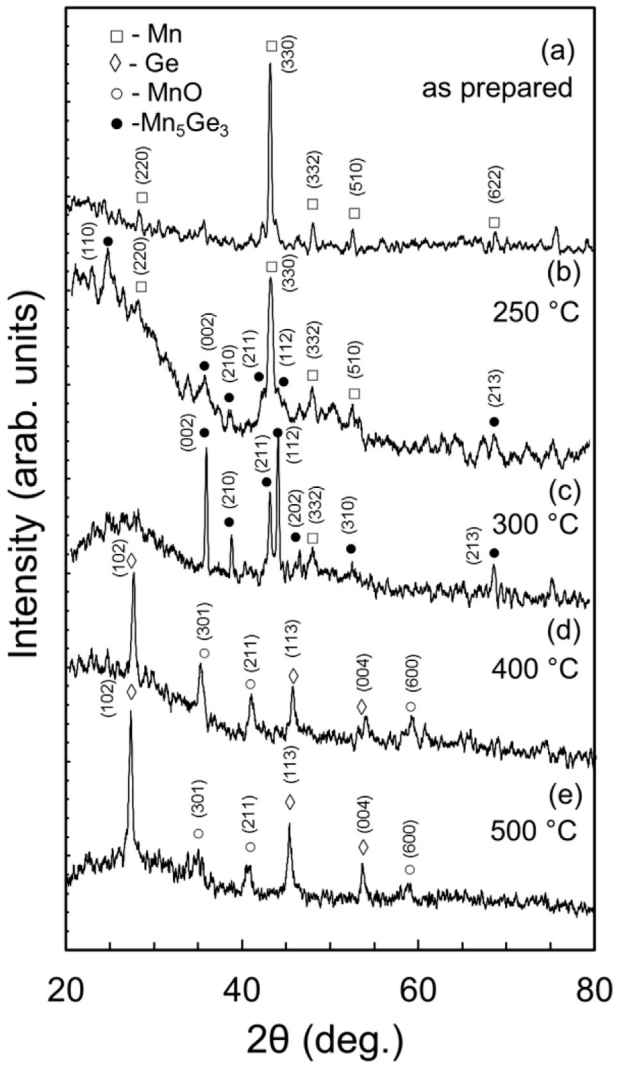


**Fig. 3.** Structural characterization of the A-Mn/GeO bilayers. X-ray diffraction patterns of the as-deposited A-Mn/GeO bilayers (a) and after annealing at 250°C (b), 300°C (c), 400°C (d), 500°C (e).

### 3.1.2. Magnetization studies

In order to characterize the magnetic properties of Mn/GeO samples after annealing at 250 °C and 300 °C the temperature dependences of the saturation magnetization $M_s$ (Fig. 4a) and hysteresis loops (Fig. 4b) of B-Mn/GeO films were measured. Both dependences indicate the formation of the $Mn_5Ge_3$ phase with a Curie temperature $T_{C1}$ ~ 300 K [14–16] and a second ferromagnetic phase with $T_{C2}$ ~ 360–400 K. Recently, we reported that in the 250–300 °C temperature interval the migration of C and O

impurity atoms into the octahedral interstitial sites of the $Mn_5Ge_3$ lattice leads to the formation of the Nowotny phase $Mn_5Ge_3C_xO_y$, with a Curie temperature $T_C$ ~350–400 K when annealing Mn/Ge bilayers [14,15] and Ge/Ag/Mn trilayers [16]. After annealing at 300 °C the magnetization increased relative to annealing at 250 °C due to the increase of the volume fraction of the $Mn_5Ge_3$ and $Mn_5Ge_3O_y$ nanoclusters in the sample. This is in good agreement with X-ray studies which show an increase in the intensity of the $Mn_5Ge_3$ reflections after annealing at 300 °C (Fig. 3b and c). Table 1 compares well-known $Mn_5Ge_3$ materials with the values of $M_s$ and $T_C$ from the obtained $Mn_5Ge_3(Mn_5Ge_3Oy)$ films.

The measurements of the perpendicular anisotropy constant $K\perp = 2\pi M_s^2 \pm \Delta K\perp$ using a torque method show that $\Delta K\perp$ ~0, which indicates the lack of in-plane strains and a grain growth texture in the $Mn_5Ge_3(Mn_5Ge_3O_y)$ nanoclusters. Hysteresis loops after annealing at both 250 °C and 300 °C (Fig. 4b) possess the ratio $M_r/M_s = 0.55$ (where $M_r$ is magnetic remanence) similar to the Stoner–Wolfarth curve with $M_r/M_s = 0.5$, which describes a random assembly of noninteracting single-domain ferromagnetic particles with uniaxial anisotropy [27]. It is known that the magnetocrystalline anisotropy constant for $Mn_5Ge_3$ $K_1 = 3.0 \times 10^5$ erg/cm$^3$ [28] and the exchange stiffness parameter $A_{ex} = 1.4 \times 10^{-7}$ erg/cm [29], which therefore implies that the exchange length $L_{ex} = (A_{ex}/K_1)^{1/2}$ is ~6.8 nm. From a magnetic point of view, it follows that the $Mn_5Ge_3(Mn_5Ge_3O_y)$ nanoclusters separated by a distance of less than 6.8 nm are exchange-coupled with each other and form Stoner-Wohlfarth particles.

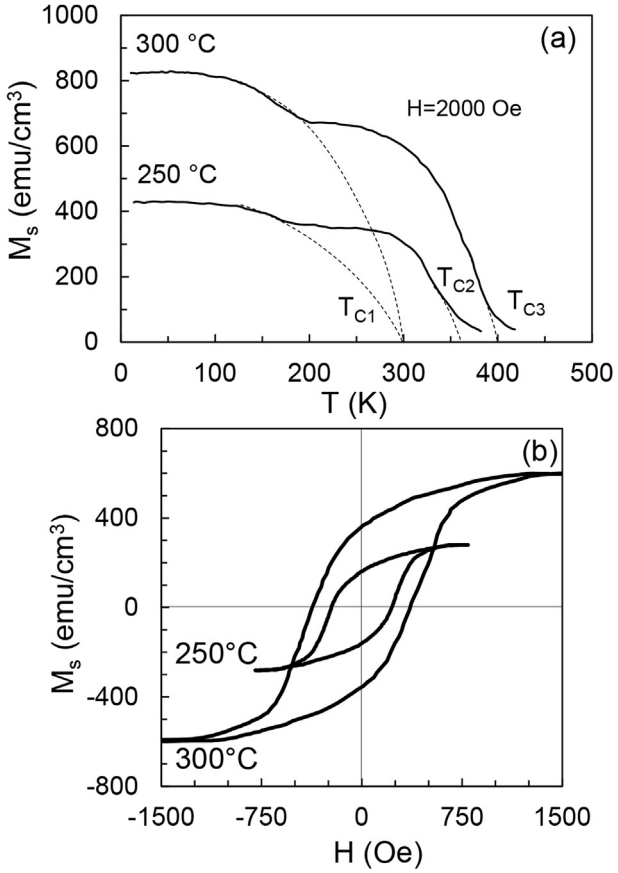


**Fig. 4.** Temperature dependence of the saturation magnetizations of $Mn_5Ge_3(Mn_5Ge_3O_y)$-$GeO_2(GeO_x)$ nanocomposite films. (a) Temperature dependences of the saturation magnetization $M_s$ measured for the B-Mn/GeO bilayer after annealing at 250 °C, and 300 °C, have clearly demonstrated the existence of the $Mn_5Ge_3$ ($T_C$ ~ 300 K) and Nowotny $Mn_5Ge_3O_y$ ($T_C$ ~ 360–400 K) ferromagnetic phases. (b) Hysteresis loops of the B-Mn/GeO bilayer after annealing at 250 °C, and 300 °C. Both hysteresis loops are consistent with the Stoner-Wohlfarth model, where the $Mn_5Ge_3(Mn_5Ge_3O_y)$ nanoclusters form a set of noninteracting uniaxial particles with randomly oriented easy axes.

Thus, magnetic studies of the B-Mn/GeO samples suggest that the final products of reactions (1), (2) contain an ensemble of noninteracting Stoner-Wohlfarth particles which are separated by a distance of more than 6.8 nm and embedded into a germanium oxide matrix.

### 3.1.3. Cross section TEM studies

Cross-sectional studies were performed in order to better understand the origin of the formation of ferromagnetic $Mn_5Ge_3$ ($Mn_5Ge_3Oy$)-$GeO_2$(GeOx) nanocomposites in the A-Mn/GeO bilayer during annealing up to 500 °C. Fig. 5 shows the cross-sectional TEM images for the initial Mn(50 nm)/Ge(300 nm) bilayer (a) and after annealing at 200 °C (b), and 300 °C (c). The initial Mn/GeO bilayer structure is clearly illustrated by TEM (Fig. 5a). EDS results reveal a homogeneous distribution of Mn and Ge in the Mn(50 nm) and GeO(300 nm) layers, respectively, (these results are not given) and this is consistent with XRD data (Fig. 3a). However, after annealing up to 500 °C the EDS elemental mapping reveals the inhomogeneous Mn, Ge and O distribution along perpendicular directions of the Mn/GeO interface. After annealing at 200 °C (Fig. 5b) and 300 °C (Fig. 5c) the cross-sectional TEM images were conditionally divided in to three layers and in Table 2 the average distributions of Mn, Ge and O are given. The analysis of the Mn, Ge and O distributions (Table 2) does not show a Mn migration into the GeO layer but instead suggests a Ge migration into the Mn layer. The TEM image of the Mn(50 nm)/GeO(300 nm) film after annealing at 300 °C (Fig. 5c) reliably demonstrates the doubling of the Mn-based layer thickness due to the migration of a considerable quantity of Ge atoms which arises due to reaction (1) in the Mn layer. This finding agrees well with our previous studies and suggests that Ge is the dominant diffusing species in the $Mn_5Ge_3$ synthesis [16]. An increase in the annealing temperature up to 500 °C leads to the oxidation of the $Mn_5Ge_3$ and Nowotny $Mn_5Ge_3Oy$ nanoclusters and further increases in the Mn-based layer as shown in Fig. 5. The cross section results affirm the XRD and magnetic data that the formation of the ferromagnetic $Mn_5Ge_3$ and Nowotny $Mn_5Ge_3Oy$ phases in the reaction products occurs after annealing at 300 °C.

The results of the cross section studies complete the XRD and magnetic data and suggest that the reaction in Mn/GeO starts with the disproportionation reaction (1), producing elementary $Ge^0$, which migrates into the Mn layer and forms the ferromagnetic $Mn_5Ge_3$ and Nowotny $Mn_5Ge_3O_y$ nanoclusters. Above 300 °C, as a result of the oxidative activity of manganese, $Mn_5Ge_3$ and $Mn_5Ge_3O_y$ decompose into a mixture of semiconductor $Ge^0$ and dielectric MnO components.

### 3.1.4. TEM characterizations

The Mn(20 nm)/GeO(30 nm) films were used to obtain further insight into the structural differences in the formation of $Mn_5Ge_3(Mn_5Ge_3O_y)$ nanoclusters in A-Mn/GeO and B-Mn/GeO

**Table 1**
Comparative data of the phases $Mn_5Ge_3$, $Mn_5Ge_3C_x$, $Mn_5Ge_3C_xO_y$, and $Mn_5Ge_3$ ($Mn_5Ge_3O_y$) obtained in this paper.

| Phase | $M_s$ (emu/cm$^3$) | $T_c$ (K) |
|---|---|---|
| $Mn_5Ge_3$ | 200 [8,9] | 300 [8,9] |
| $Mn_5Ge_3C_x$ | 600 [8,9] | 460 [8,9] |
| $Mn_5Ge_3C_xO_y$ | 250 [16] | 400 [16] |
| $Mn_5Ge_3$ ($Mn_5Ge_3O_y$) | 600 [this work] | 400 [this work] |

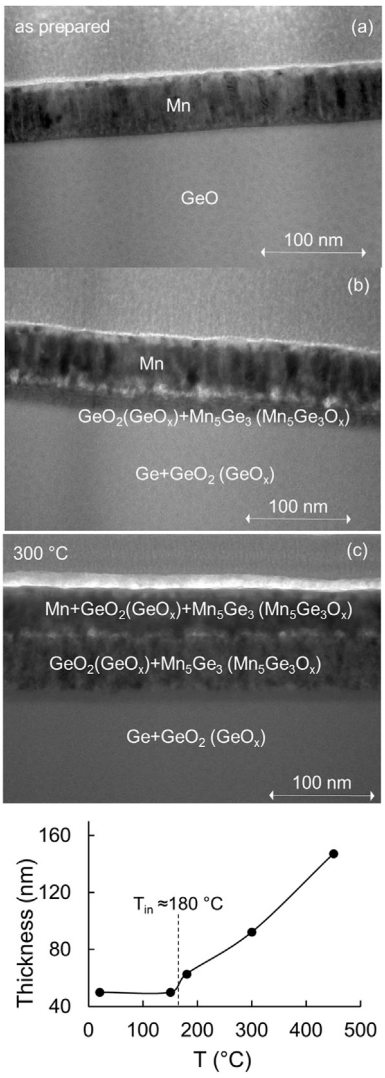


**Fig. 5.** A direct evidence of the low-temperature synthesis of $Mn_5Ge_3(Mn_5Ge_3O_y)$-$GeO_2(GeO_x)$ in A-Mn/GeO bilayers. TEM image of the cross-section of the A-Mn/GeO bilayers: (a) as-deposited, (b) after annealing at 200 °C and (c) 300 °C. After annealing above 180 °C the GeO undergoes disproportion and $Mn_5Ge_3(Mn_5Ge_3O_y)$-$GeO_2(GeO_x)$ nanostructures are formed at the Mn/GeO interface. The EDS element mapping of the Mn, O and Ge in layers of the as-deposited and after annealing at 200 °C and 300 °C samples are presented in Table 2. (d) The thickness of the reaction product layer as a function of the annealing temperature up to 500 °C.

**Table 2**
The EDS element mapping of the Mn, O and Ge of the as-deposited (a) and after annealing at 200 °C (b) and 300 °C (c) A-Mn/GeO bilayers.

| N⁰ | Layer | Chemical elements (at.%) | | |
|---|---|---|---|---|
| | | Mn | Ge | O |
| (a) | Mn | 99 | 0 | 1 |
| | GeO | 0 | 50 | 50 |
| (b) | Mn | 98 | 0 | 2 |
| | $GeO_2(GeO_x)$+ $Mn_5Ge_3$ ($Mn_5Ge_3O_x$) | 60 | 42 | 8 |
| | $Ge+GeO_2(GeO_x)$ | 0 | 50 | 50 |
| (c) | $Mn+GeO_2(GeO_x)+Mn_5Ge_3$ ($Mn_5Ge_3O_x$) | 60 | 35 | 5 |
| | $GeO_2(GeO_x)$+ $Mn_5Ge_3$ ($Mn_5Ge_3O_x$) | 30 | 60 | 10 |
| | $Ge+GeO_2(GeO_x)$ | 0 | 50 | 50 |

samples during annealing up 300 °C. Fig. 6 shows a typical TEM image (**a**) and the selected area electron diffraction pattern (SAED) (**b**) of the B-Mn/GeO film after annealing at 300 °C. The average atomic numbers for the $GeO_x$ and $GeO_2$ phases are lower than the atomic numbers of Mn and Ge, thus the GeO and $GeO_2$ regions appears brighter than the Mn region on the TEM image (Fig. 6a). The d-spacing obtained from the SAED pattern (Fig. 6b) indicates the possible presence of a MnO phase besides the expected $Mn_5Ge_3$ and $Mn_5Ge_3O_y$ phases, as illustrated in Table 3. Fig. 6c, shows the part of the SEM image on which EDS analysis was done. Elemental maps in Fig. 6d and e reveal that Ge and Mn are the elemental constituents of the $Mn_5Ge_3(Mn_5Ge_3O_y)$ nanocomposite material. The elemental mapping of Ge, as seen in Fig. 6d, reveals an increased concentration of Ge in two large nanoparticles and is quite homogeneous in the rest of the study area. The mapping of Mn is shown in Fig. 6e, which demonstrated that all of the Mn is distributed homogeneously. The TEM observations (Fig. 6a,c) indicate that the Ge-rich nanoparticles have an out-of-round shape with a grain size of 50–80 nm and intercluster distances of 150–300 nm and good uniformity in the reaction product. It is important to bear in mind that nanoparticles with a size below 20 nm are not observed in the TEM image. Since the B-Mn/GeO films become ferromagnetic after annealing at 300 °C, it follows that the size of the $Mn_5Ge_3(Mn_5Ge_3O_y)$ nanoparticles is less than 20 nm. Typical ferromagnetic nanoparticles with a size below 20 nm are in the superparamagnetic state and do not exhibit a magnetic hysteresis loop. However, the appearance of hysteresis loops (Fig. 4b) suggests that the $Mn_5Ge_3(Mn_5Ge_3O_y)$ nanoparticles are separated by distances less than the exchange length $L_{ex} = 6.8$ nm and are exchange-coupled with each other through the $GeO_2(GeO_x)$ matrix. The aggregations of these $Mn_5Ge_3$ ($Mn_5Ge_3O_y$) nanoparticles can be considered as a Stoner-Wohlfarth ensemble of noninteracting particles, which exhibit a magnetic hysteresis loop (Fig. 4b).

Thus, these results indicate the creation of nanocomposites in the B-Mn/GeO samples that largely consist of very small $Mn_5Ge_3(Mn_5Ge_3O_y)$ nanoparticles with dimensions less than 20 nm and a small number of Ge-rich nanoparticles with sizes of 50–80 nm embedded into the $GeO_2(GeO_x)$ matrix. Based on these findings, we suppose that the interface layer in the A-Mn/GeO samples (Fig. 5c) is the same as the B-Mn/GeO layers and contains

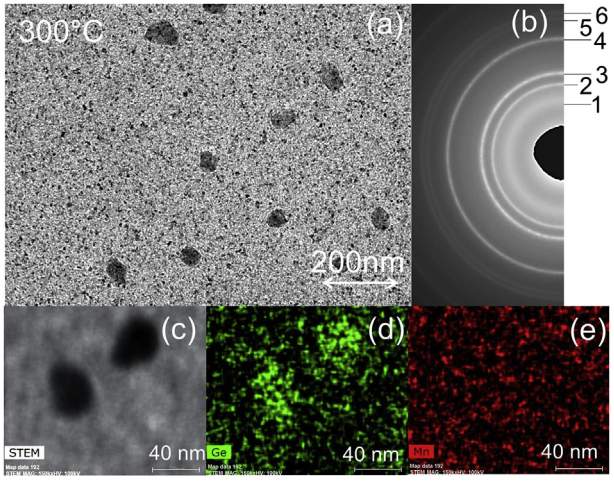


**Fig. 6.** (a) TEM image, (b) SAED pattern of the $Mn_5Ge_3$ ($Mn_5Ge_3O_y$)-$GeO_2(GeO_x)$ film after annealing of B-Mn/GeO bilayers at 300 °C, (c) TEM image area of elemental mapping, (d) Ge element mapping, (e) Mn element mapping. The TEM and Ge element mapping, show the presence of Ge-rich nanoparticles in the B-Mn/GeO bilayers after annealing at 300 °C.

**Table 3**
Indexing the diffraction reflections SAED pattern of the $Mn_5Ge_3$($Mn_5Ge_3Oy$)-$GeO_2$(GeOx) film after annealing at 300 °C in (Fig. 6b).

| № | $Mn_5Ge_3$ | NaCl | MnO |
|---|---|---|---|
| 1 | – | 200 | – |
| 2 | 211 | – | 200 |
| 3 | 112 | 220 | – |
| 4 | 202 | – | 311 |
| 5 | 213 | – | – |
| 6 | 331 | – | – |

$Mn_5Ge_3$($Mn_5Ge_3O_y$) nanoparticles in a $GeO_2$($GeO_x$) matrix. The TEM studies show the formation of ferromagnetic $Mn_5Ge_3$($Mn_5Ge_3O_y$)-$GeO_2$($GeO_x$) films, from which it follows that an easy way to fabricate $Mn_5Ge_3$($Mn_5Ge_3O_y$)-$GeO_2$($GeO_x$) nanocomposite films of different thicknesses is by annealing the $(B\text{-}Mn/GeO)_n$ multilayers at 300 °C.

### 3.2. Structural evolution of GeO films upon thermal annealing

#### 3.2.1. Thermal annealing effect on optical properties of GeO thin films

To understand the reaction mechanism between Mn and GeO the decomposition of amorphous GeO into Ge and $GeO_2$ according to reaction (1) was investigated by annealing up to 500 °C, and the schematic illustration is presented in Fig. 7a. Fig. 7b shows the optical density of as-deposited GeO, GeO after annealing at 300 °C and Ge films having a corresponding thickness excluding the contribution of a glass substrate. The optical density at wavelengths ranging from 300 to 900 nm of the as-deposited Ge and GeO after annealing at 300 °C almost coincide. The minor difference between them is the result of the presence of $GeO_2$ in the annealed sample. The dependence of the optical density at 400 nm of as-deposited GeO film as a function of annealing temperature is presented in Fig. 7c. Optical density of GeO film does not change up to ~180 °C, which evidences the lack of phase transformations in GeO film. The strong increase in the optical density above 180 °C clearly demonstrates the onset of the disproportionation reaction (1) with the initiation temperature $T_{in} = 180$ °C. The highest amount of released elemental $Ge^0$ in the annealed ($Ge^0$+$GeO_2$) sample is reached at a temperature of 300 °C; this is evident from the maximization of the optical density at a wavelength of 400 nm (Fig. 7c). As can be seen from Fig. 7c, further increases in the annealing temperature above 300 °C leads to a decrease of the optical density which approaches zero at 500 °C. This indicates the complete oxidation of germanium at 500 °C and the formation of $GeO_2$, which has a high transparency in the visible range. Our findings are in good agreement with previously published results of the formation of Ge nanoclusters in GeO film by annealing [30–35] and an important contribution is the detection of the low initiation temperature $T_{in} = 180$ °C of reaction (1).

#### 3.2.2. XPS of as-deposited of GeO and after annealing at 300 °C

Fig. 8a shows the photoelectron Ge 3d spectra of as-deposited GeO film (1, 2) and the film annealed at 300 °C (3, 4) collected before (1, 3) and after etching with $Ar^+$ ions (2, 4). The binding energy of the main Ge 3d peak at ~31 eV, and the O/Ge atomic ratio, which was somewhat higher than 1 and decreased to 1 after $Ar^+$ etching, indicate that a nearly stoichiometric GeO oxide was fabricated in the as-deposited sample; some enrichment of the surface with oxygen was due to the outermost $GeO_2$ which is inevitably produced after exposure to the atmosphere [36] (Fig. 8b, Supplementary Table S1). The spectrum from the sample annealed at 300 °C (Fig. 8a) contained contributions with binding energies of

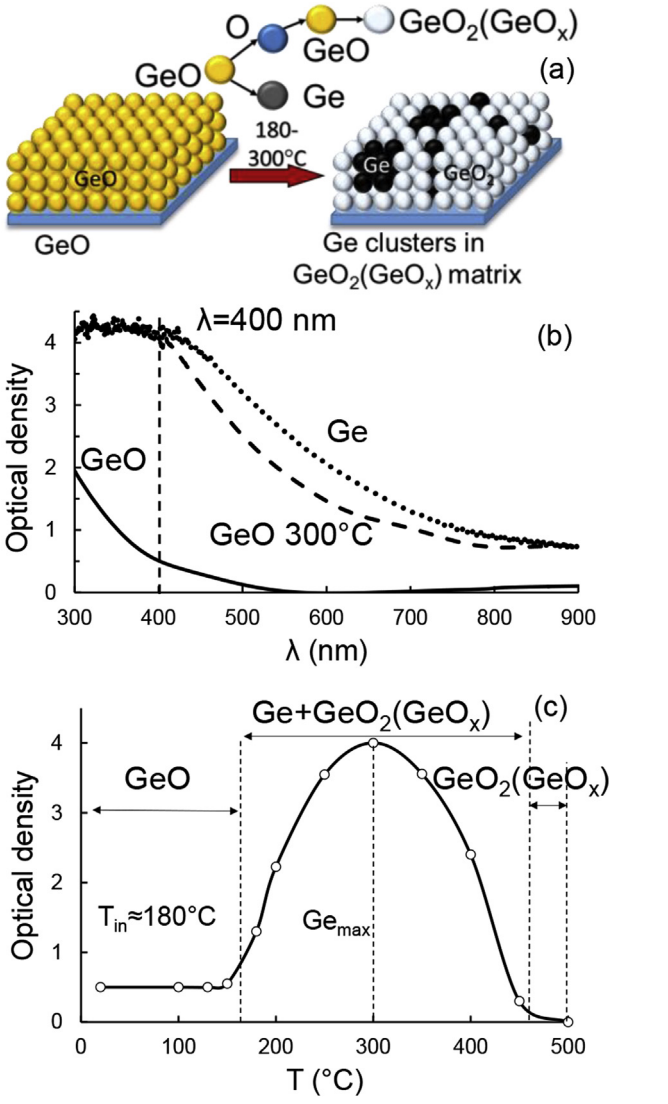


**Fig. 7.** (a) Schematic illustration of the disproportional reaction (1), including the start at 180 °C and the increase up to 300 °C in the volume fraction of the Ge nanoclusters embedded in the Ge oxide matrix. (b) Comparison of optical spectra of as-deposited GeO film (solid), GeO after annealing at 300 °C (dashed line) and Ge film having a corresponding thickness (dotted line); contribution of glass substrate is extracted from all spectra. The optical densities of Ge and GeO after annealing at 300 °C coincide at 400 nm, therefore this wavelength was used for finding the dependence given in (c). (c) The dependence of the optical density at 400 nm of as-deposited GeO film as a function of annealing temperature. The maximal increase of the optical density at 300 °C means a maximal content of Ge nanoclusters in the sample, and a strong decrease of optical density above 400 °C means the oxidation of Ge to $GeO_2$.

32.6, 30.7, and 29.5 eV, which correspond to $GeO_2$, GeO, and metallic $Ge^0$, respectively [37,38]. This corroborates with the disproportionation of GeO via reaction (1). For both samples, the $Ar^+$ sputtering largely removed the surface $GeO_2$ and any excessive oxygen so the atomic O/Ge ratio approached ~1 but also caused the additional decomposition of GeO and shifts of the $Ge^{2+}$ peaks due to the formation of the non-stoichiometric oxides $GeO_{1-x}$ and $GeO_{1+x}$ [36–38] (Fig. 8a). Similar trends can also be monitored in the O 1s spectra (Supplementary Fig. S1, Supplementary Table S1).

Thus, the XPS findings agree with the assumption that the as-deposited films were composed of GeO oxide, which disproportionates above 180 °C, and the reaction products were Ge nanoclusters embedded into a $GeO_2$($GeO_x$) matrix.

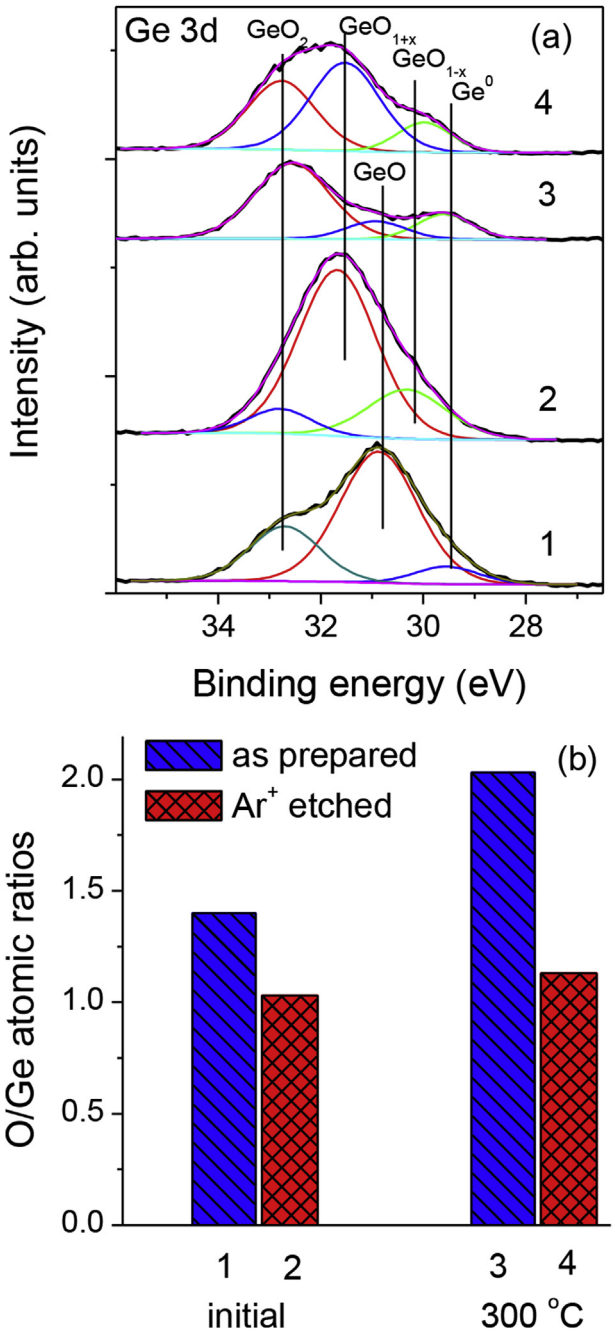


**Fig. 8.** (a) X-ray photoelectron Ge 3d spectra of as-prepared GeO film (1,2) and the nanocomposite Ge-$GeO_2$($GeO_x$) film annealed at 300°C (3,4). (b) Relative concentrations of Ge and O derived from the XPS; the data suggest that the reaction products also contain substoichiometric $GeO_x$ in addition to GeO, $GeO_2$ and Ge.

### 3.2.3. TEM images

Fig. 9 shows a typical TEM image of the as-deposited GeO film and after annealing at 300 °C. The initial GeO films possessed a sand-like microstructure, which indicates that the size of the GeO nanograins is very small (<5 nm) (Fig. 9a). The average atomic numbers for the $GeO_2$ and $GeO_x$ phases are lower than the atomic number of Ge, thus the $GeO_2$ and $GeO_x$ region appears brighter than the Ge region on the TEM image (Fig. 9b) and EDS analysis confirms that the observed nanoparticles are germanium rich. After annealing at 300 °C the TEM image clearly shows the formation of Ge nanoparticles of out-of-round shape with an average grain size

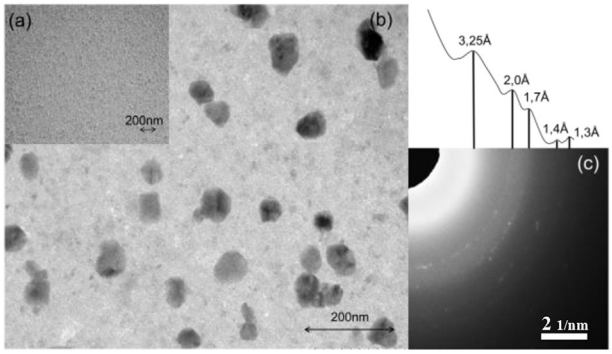


**Fig. 9.** (a) TEM image of as-deposited GeO film, (b) TEM image and **(c)** the corresponding SAED pattern of the GeO film after annealing at 300 °C. The TEM and SAED data confirms the presence of Ge nanocrystals in the uniform amorphous $GeO_2$($GeO_x$) matrix established on the basis of EDS and XPS analysis.

of ~60 nm and these findings are in good agreement with previously published results [34,35]. It is important to note that the constituent part of Ge nanoparticles has a size below 20 nm, which is not observed in the TEM image. Fig. 9c shows the SAED pattern of the GeO film after annealing at 300 °C which exhibited faint diffraction rings corresponding to d-spacing of 3.25, 2.0, 1.7 and 1.3 Å, which represent diffraction from the (111), (220), (311), (331) planes of Ge and there are no reflections from either $GeO_2$ or $GeO_x$. This clearly confirm the synthesis of polycrystalline Ge nanocrystals in an amorphous $GeO_2$($GeO_x$) matrix.

Thus, the XPS and TEM observations indicate that the as-deposited films were stoichiometric GeO oxides, which undergo the disproportionation reaction (1) above the initiation temperature ~ 180 °C, and after annealing at 300 °C the reaction products were Ge nanoclusters with an average diameter ~ 60 nm embedded into a $GeO_2$($GeO_x$) matrix.

## 4. Discussion

From magnetic measurements it follows that the anomalous part of the perpendicular anisotropy constant $\Delta K^{\perp}$ ~0. Consequently, the increase of $T_C$ in $Mn_5Ge_3O_y$ nanoclusters cannot be explained by the effect of in-plane strains and the grain growth texture. The similarity of temperature dependences of the magnetization curves and the insignificant difference in the Curie temperatures $T_C$ of the $Mn_5Ge_3$ ($Mn_5Ge_3O_y$) and C-doped $Mn_5Ge_3C_x$ films indicate a general mechanism of an increase of $T_C$ compared to the $Mn_5Ge_3$ samples. This suggests that, similar to how C modifies the electronic structure of C-doped $Mn_5Ge_3C_x$ [12,13], the exchange interaction initiated by the intermediate O-ions between $Mn_{II}$-$Mn_{II}$ in $Mn_5Ge_3O_y$ increases the $T_C$ value. These assumptions can explain the differences in $T_C$ for $Mn_5Ge_3O_y$ films between annealing temperatures of 250 °C and 300 °C (Fig. 4a). Increasing the temperature increases the rates of reactions (1), (2) and the migration of oxygen atoms into the interstitial voids of the $Mn_{II}$ octahedra. This leads to an increase of the oxygen concentration in the $Mn_5Ge_3O_y$ nanoclusters and consequently, an increase of $T_C$ up to ~360 K and ~400 K after annealing at 250 °C and ~300 °C, respectively. This is in good agreement with increase of $T_C$ up to ~370 K and ~430 K in $Mn_5Ge_3C_x$ when the carbon concentration reaches values of $x = 0.1$ and $x = 0.6$, respectively [13]. This assumption also agrees with the increase of $T_C$ in sputtered $Mn_5Ge_3$ layers containing C and O impurities produced by the reactive diffusion of Mn and Ge layers [2,14,15] and in dilute $Ge_{1-x}Mn_x$ amorphous thin films grown by molecular beam epitaxy on a Ge (001) substrate [17].

As is known, thin-film solid-state reactions start when the

temperature of a sample $T_s$ exceeds the initiation (formation) temperature $T_{in}(T_s > T_{in})$. For metallic thin-film reactions the initiation temperature $T_{in}$ can be below room temperature or even below 90 K [16,39]. Recently we showed that the initiation temperature of the $Mn_5Ge_3$ compound is equal to $T_{in}(Mn_5Ge_3) \sim 120\,^{\circ}C$ [14–16] and the Ge is the sole diffusing species [16]. As pointed out above the reaction between the Mn and GeO layers starts at $T_{in}(Mn/GeO) = 180\,^{\circ}C$ which coincides with the initiation temperature $T_{in}(GeO \rightarrow Ge + GeO_2) = 180\,^{\circ}C$ of the disproportionation reaction (1) that produces Ge and $GeO_2$, which exceeds the initiation temperature of $Mn_5Ge_3$ ($T_{in}$ ~120 °C). This result and the analysis of magnetic and structural data propose the hypothesized scenario for the synthesis of $Mn_5Ge_3 - GeO_2$ nanocomposite films. As the annealing temperature in the (Mn/GeO) bilayer increases above 180 °C due to reaction (1) the GeO decomposes into elemental oxygen and germanium, which uniformly occur throughout the entire volume of the GeO film. At the same time strong chemical interactions arise between the Mn and Ge atoms and, because Ge is the sole diffusing species, the Ge atoms migrate directly into the Mn layer via the Mn/GeO interface and form $Mn_5Ge_3$ nanoclusters with sizes less than 20 nm. However, Ge nanoclusters arising far from the Mn/GeO interface can grow, reaching 50–80 nm (Fig. 6a,c). An important point is that the same nanoclusters are formed in GeO films after annealing at 300 °C (Fig. 9b). The oxygen released during reaction (1) not only participates in the synthesis of the Ge oxides ($GeO_x$, $GeO_2$), but also migrates into the $Mn_5Ge_3$ lattice and forms Nowotny $Mn_5Ge_3O_y$ nanoclusters. Above 300 °C Mn is oxidized and forms a stable MnO oxide. As a consequence of this the $Mn_5Ge_3$ and $Mn_5Ge_3O_y$ decomposes into elemental Ge and MnO and after annealing above 450 °C the reaction products contain Ge, MnO, $GeO_x$ and $GeO_2$ phases.

Our results demonstrate the important role of oxygen in the control of the magnetic properties of the $Mn_5Ge_3$-$GeO_2$ nanocomposites. These nanocomposites combine both the magnetic properties of the $Mn_5Ge_3$ and $Mn_5Ge_3O_y$ nanoclusters and the dielectric characteristics of the $GeO_x$ and $GeO_2$ oxides, providing a new room-temperature functional material.

## 5. Conclusion

To summarize, the solid-state reactions in the Mn/GeO bilayers were investigated in the temperature range from 50 to 500 °C. The mixing of the Mn and GeO layers and the synthesis of the ferromagnetic $Mn_5Ge_3$ and $Mn_5Ge_3O_y$ phases at the Mn/GeO interface start above the initiation temperature $T_{in}$ ~180 °C and the $Mn_5Ge_3$ and $Mn_5Ge_3O_y$ fraction volume increase after annealing up to 300 °C. Although the actual scenarios for the migration of oxygen atoms to the $Mn_5Ge_3$ lattice remain unknown, the analogous temperature dependences of the saturation magnetizations and the close Curie temperatures clearly indicate the same mechanisms for increasing the Curie temperature in the $Mn_5Ge_3C_x$ and $Mn_5Ge_3O_y$ films. Annealing above 300 °C leads to the oxidation of Mn in the $Mn_5Ge_3$ and $Mn_5Ge_3O_y$ nanoclusters with the formation of the MnO and elemental Ge and Ge oxides. Furthermore, the thin-film solid-state Mn/GeO reactions can be considered as a low-temperature technique to synthesize high-Curie temperature and high magnetization $Mn_5Ge_3(Mn_5Ge_3O_y)$-$GeO_2(GeO_x)$ nanocomposite films.

## Acknowledgements

This study was supported by the Russian Foundation for Basic Research (grants #18-02-00779, #16-03-00069, #17-52-53031), by Russian foundation for basic research, government of Krasnoyarsk territory, Krasnoyarsk Region science and technology support fund to research project # 18-42-243009 р_мол_а, by the council for grants of the president of Russian federation (SP-1373.2016.3). The XPS and TEM studies were carried out using the facilities of Performance service at Krasnoyarsk Scientific Center.

## Appendix A. Supplementary data

Supplementary data to this article can be found online at https://doi.org/10.1016/j.jallcom.2018.12.126.

## References

[1] R. Kalvig, E. Jedryka, P. Aleshkevych, M. Wojcik, W. Bednarski, M. Petit, L. Michez, Ferromagnetic resonance in $Mn_5Ge_3$ epitaxial films with weak stripe domain structure, J. Phys. D Appl. Phys. 50 (2017), 125001-1 - 125001-9.
[2] E. Assaf, A. Portavoce, K. Hoummada, M. Bertoglio, S. Bertaina, High Curie temperature $Mn_5Ge_3$ thin films produced by non-diffusive reaction, Appl. Phys. Lett. 110 (2017), 072408-1 - 072408-4.
[3] T. Toliński, K. Synoradzki, Specific heat and magnetocaloric effect of the $Mn_5Ge_3$ ferromagnet, Intermetallics 47 (2014) 1–5.
[4] Y.K. Wakabayashi, R. Akiyama, Y. Takeda, M. Horio, G. Shibata, S. Sakamoto, Y. Ban, Y. Saitoh, H. Yamagami, A. Fujimori, M. Tanaka, S. Ohya, Origin of the large positive magnetoresistance of $Ge_{1-x}Mn_x$ granular thin films, Phys. Rev. B 95 (2017), 014417-1 - 014417-6.
[5] C. Sürgers, G. Fischer, P. Winkel, H.v. Löhneysen, Magnetotransport in ferromagnetic $Mn_5Ge_3$, $Mn_5Ge_3C_{0.8}$ and $Mn_5Si_3C_{0.8}$ thin films, Phys. Rev. B 90 (2014), 104421-1 - 104421-9.
[6] R.P. Panguluri, C. Zeng, H.H. Weitering, J.M. Sullivan, S.C. Erwin, B. Nadgorny, Spin polarization and electronic structure of ferromagnetic $Mn_5Ge_3$ epilayers, Phys. Status Solidi (b) 242 (2005) R67–R69.
[7] Yu. S. Dedkov, M. Holder, G. Mayer, M. Fonin, A.B. Preobrajenski, Spin-resolved photoemission of a ferromagnetic $Mn_5Ge_3$(001) epilayer on Ge(111), J. Appl. Phys. 105 (2009), 073909-1 - 073909-4.
[8] V.L. Thanh, A. Spiesser, M.-T. Dau, S.F. Olive-Mendez, L.A. Michez, M. Petit, Epitaxial growth and magnetic properties of $Mn_5Ge_3$/Ge and $Mn_5Ge_3C_x$/Ge heterostructures for spintronic applications, Adv. Nat. Sci. Nanosci. Nanotechnol. 4 (2013), 043002-1 - 043002-9.
[9] M. Petit, L. Michez, C.-E. Dutoit, S. Bertaina, V.O. Dolocan, V. Heresanu, M. Stoffel, V.L. Thanh, Very low-temperature epitaxial growth of $Mn_5Ge_3$ and $Mn_5Ge_3C_{0.2}$ films on Ge(111) using molecular beam epitaxy, Thin Solid Films 589 (2015) 427–432.
[10] A. Alvídrez-Lechuga, R. López Antón, J. Trinidad Holguín-Momaca, F. Espinosa-Magaña, S. Federico Olive-Méndez, Role of the substrate temperature on the growth of Mn5Ge3 thin films by co-deposition of Mn and Ge on Ge(001) substrates by magnetron sputtering, Thin Solid Films 616 (2016) 111–115.
[11] S. Yada, P.N. Hai, S. Sugahara, M. Tanaka, Structural and magnetic properties of $Ge_{1-x}Mn_x$ thin films grown on Ge (001) substrates, J. Appl. Phys. 110 (2011), 073903-1 - 073903-8.
[12] M. Gajdzik, C. Sürgers, M.T. Kelemen, H.V. Löhneysen, Strongly enhanced Curie temperature in carbon-doped Mn5Ge3 films, J. Magn. Magn. Mater. 221 (2000) 248–254.
[13] A. Spiesser, I. Slipukhina, M.-T. Dau, E. Arras, V. Le Thanh, L. Michez, P. Pochet, H. Saito, S. Yuasa, M. Jamet, J. Derrien, Control of magnetic properties of epitaxial $Mn_5Ge_3C_x$ films induced by carbon doping, Phys. Rev. B 84 (2011), 165203-1 - 165203-7.
[14] V.G. Myagkov, V.S. Zhigalov, A.A. Matsynin, L.E. Bykova, Yu.L. Mikhlin, G.N. Bondarenko, G.S. Patrin, G.Yu. Yurkin, Formation of ferromagnetic germanides by solid-state reactions in 20Ge/80Mn films, Thin Solid Films 552 (2014) 86–91.
[15] V.G. Myagkov, V.S. Zhigalov, A.A. Matsynin, L.E. Bykova, G.V. Bondarenko, G.N. Bondarenko, G.S. Patrin, D.A. Velikanov, Phase transformations in the Mn-Ge system and in $Ge_xMn_{1-x}$ diluted semiconductors, JETP Lett. 96 (2012) 40–43.
[16] V.G. Myagkov, L.E. Bykova, A.A. Matsynin, M.N. Volochaev, V.S. Zhigalov, I.A. Tambasov, Yu.L. Mikhlin, D.A. Velikanov, G.N. Bondarenko, Solid state synthesis of $Mn_5Ge_3$ in Ge/Ag/Mn trilayers: structural and magnetic studies, J. Solid State Chem. 246 (2017) 379–387.
[17] W. Yin, C.D. Kell, L. He, M.C. Dolph, C. Duska, J. Lu, R. Hull, J.A. Floro, S.A. Wolf, Enhanced magnetic and electrical properties in amorphous Ge: Mn thin films by non-magnetic codoping, J. Appl. Phys. 111 (2012), 033916-1 - 033916-7.
[18] S. Tardif, S. Cherifi, M. Jamet, T. Devillers, A. Barski, D. Schmitz, N. Darowski, P. Thakur, J.C. Cezar, N.B. Brookes, R. Mattana, J. Cibert, Exchange bias in GeMn nanocolumns: the role of surface oxidation, Appl. Phys. Lett. 97 (2010), 062501-1- 062501-3.
[19] B. Toydemir, A.C. Onel, M. Ertas, L. Colakerol Arslan, Role of nitrogen on the magnetic properties of MBE grown Mn0.04Ge0.96 films, J. Magn. Magn. Mater. 393 (2015) 220–225.
[20] P. De Padova, J.-P. Ayoub, I. Berbezier, J.-M. Mariot, A. Taleb-Ibrahimi, M.C. Richter, O. Heckmann, A.M. Testa, D. Fiorani, B. Olivieri, S. Picozzi, K. Hricovini, MnxGe1–x thin layers studied by TEM, X-ray absorption

spectroscopy and SQUID magnetometry, Surf. Sci. 601 (2007) 2628–2631.
[21] A. Continenza, G. Profeta, Role of oxygen defects in diluted Mn:Ge, Phys. Rev. B 78 (2008), 085215-1 - 085215-7.
[22] K. Sato, T. Mizoguchi, Simple analysis of torque measurement of magnetic thin films, J. Appl. Phys. 47 (1976) 4669–4671.
[23] S. Chikazumi, Epitaxial growth and magnetic properties of single-crystal films of iron, nickel, and permalloy, J. Appl. Phys. 32 (1961) 81S.
[24] K. Vijayarangamuthu, S. Ratha, D. Kabiraj, D.K. Avasthi, P.K. Kulriya, V.N. Singh, B.R. Mehta, Ge nanocrystals embedded in a $GeO_x$ matrix formed by thermally annealing of Ge oxide films, J. Vac. Sci. Technol. A 27 (2009) 731–733.
[25] S.K. Wang, H.-G. Liu, A. Toriumi, Kinetic study of GeO disproportionation into a $GeO_2$/Ge system using x-ray photoelectron spectroscopy, Appl. Phys. Lett. 101 (2012), 061907-1 – 061907-4.
[26] C.J. Sahle, C. Sternemann, H. Conrad, A. Herdt, O.M. Feroughi, M. Tolan, A. Hohl, R. Wagner, D. Lützenkirchen–Hecht, R. Frahm, A. Sakko, K. Hämäläinen, Phase separation and nanocrystal formation in GeO, Appl. Phys. Lett. 95 (2009), 021910-1 – 021910-3.
[27] C. Tannous, J. Gieraltowski, The Stoner–Wohlfarth model of ferromagnetism, Eur. J. Phys. 29 (2008) 475–487.
[28] Y. Tawara, K. Sato, On the magnetic anisotropy of single crystal of Mn5Ge3, J. Phys. Soc. Jpn. 18 (1963) 773–777.
[29] L.-A. Michez, F. Virot, M. Petit, R. Hayn, L. Notin, O. Fruchart, V. Heresanu, M. Jamet, V. Le Thanh, Magnetic anisotropy and magnetic domain structure in C-doped Mn5Ge3, J. Appl. Phys. 118 (2015), 043906-1 - 043906-7.
[30] K. Vijayarangamuthu, S. Rath, D. Kabiraj, D.K. Avasthi, P.K. Kulriya, V.N. Singh, B.R. Mehta, Ge nanocrystals embedded in a GeOx matrix formed by thermally annealing of Ge oxide films, J. Vac. Sci. Technol. A 27 (2009) 731–733.
[31] C.J. Sahle, C. Sternemann, H. Conrad, A. Herdt, O.M. Feroughi, M. Tolan, A. Hohl, R. Wagner, D. Lützenkirchen–Hecht, R. Frahm, A. Sakko, K. Hämäläinen, Phase separation and nanocrystal formation in GeO, Appl. Phys. Lett. 95 (2009), 021910-1 - 021910-3.
[32] S. Kai Wang, H.-G. Liu, A. Toriumi, Kinetic study of GeO disproportionation into a $GeO_2$/Ge system using x-ray photoelectron spectroscopy, Appl. Phys. Lett. 101 (2012), 061907-1 - 061907-1.
[33] J.A. McLeod, J. Zhao, L. Yang, Y. Liu, L. Liu, Structural evolution of reduced $GeO_x$ nanoparticles, Phys. Chem. Chem. Phys. 19 (2017) 3182–3191.
[34] Y. Barta, D. Kabiraj, D. Kanjilan, Development of Ge nanoparticles embedded in $GeO_2$ matrix, J. Nanosci. Nanotechnol. 8 (2008) 4081–4085.
[35] J. Wu, L. Han, N. Wang, Y. Song, H. Chen, H. Chen, J. Hu, *In situ* structural evolution from GeO nanospheres to GeO/(Ge, $GeO_2$) core-shell nanospheres and to Ge hollow nanospheres, CrystEngComm 13 (2011) 4611–4616.
[36] S.K. Wang, H.-G. Liu, A. Toriumi, Kinetic study of GeO disproportionation into a $GeO_2$/Ge system using x-ray photoelectron spectroscopy, Appl. Phys. Lett. 101 (2012), 061907-1 – 061907-4.
[37] N.M. Bom, G.V. Soares, S. Hartmann, A. Bordin, C. Radtke, $GeO_2$/Ge structure submitted to annealing in deuterium: incorporation pathways and associated oxide modifications, Appl. Phys. Lett. 105 (2014), 141605-1 - 141605-4.
[38] T. Sasada, Y. Nakakita, M. Takenaka, S. Takagia, Surface orientation dependence of interface properties of $GeO_2$/Ge metal-oxide-semiconductor structures fabricated by thermal oxidation, J. Appl. Phys. 106 (2009), 073716-1 - 073716-7.
[39] V. Myagkov, O. Bayukov, Yu. Mikhlin, V. Zhigalov, L. Bykova, G. Bondarenko Galina, Long-range chemical interactions in solid-state reactions: effect of an inert Ag interlayer on the formation of $L1_0$-FePd in epitaxial Pd(001)/Ag(001)/Fe(001) and Fe(001)/Ag(001)/Pd(001) trilayers, Phil. Mag. 94 (2014) 2595–2622.